

Article

Surface Finish Analysis in Single Point Incremental Sheet Forming of Rib-Stiffened 2024-T3 and 7075-T6 Alclad Aluminium Alloy Panels

Tomasz Trzepieciński ^{1,*} , Andrzej Kubit ² , Andrzej Dzierwa ^{2,*} , Bogdan Krasowski ³ and Wojciech Jurczak ⁴ 

¹ Department of Materials Forming and Processing, Rzeszow University of Technology, al. Powst. Warszawy 8, 35-959 Rzeszów, Poland

² Department of Manufacturing and Production Engineering, Rzeszow University of Technology, al. Powst. Warszawy 8, 35-959 Rzeszów, Poland; akubit@prz.edu.pl

³ Department of Mechanics and Machine Building, Carpatian State School in Krosno, ul. Żwirki i Wigury 9A, 38-400 Krosno, Poland; bogdan.krasowski@kpu.krosno.pl

⁴ Faculty of Mechanical and Electrical Engineering, Polish Naval Academy, ul. Śmidowicza 69, 81-127 Gdynia, Poland; w.jurczak@amw.gdynia.pl

* Correspondence: tomtrz@prz.edu.pl (T.T.); adzierwa@prz.edu.pl (A.D.)

Abstract: The article presents the results of the analysis of the interactions between the single point incremental forming (SPIF) process parameters and the main roughness parameters of stiffened ribs fabricated in Alclad aluminium alloy panels. EN AW-7075-T6 and EN AW-2024-T3 Alclad aluminium alloy sheets were used as the research material. Panels with longitudinal ribs were produced with different values of incremental vertical step size and tool rotational speed. Alclad is formed of high-purity aluminium surface layers metallurgically bonded to aluminium alloy core material. The quality of the surface roughness and unbroken Alclad are key problems in SPIF of Alclad sheets destined for aerospace applications. The interactions between the SPIF process parameters and the main roughness parameters of the stiffened ribs were determined. The influence of forming parameters on average roughness Sa and the 10-point peak–valley surface roughness Sz was determined using artificial neural networks. The greater the value of the incremental vertical step size, the more prominent the ridges found in the inner surface of stiffened ribs, especially in the case of both Alclad aluminium alloy sheets. The predictive models of ANNs for the Sa and the Sz were characterised by performance measures with R^2 values lying between 0.657 and 0.979. A different character of change in surface roughness was found for sheets covered with and not covered with a soft layer of technically pure aluminium. In the case of Alclad sheets, increasing the value of the incremental vertical step size increases the value of the surface roughness parameters Sa and Sz . In the case of the sheets not covered by Alclad, reduction of the tool rotational speed increases the Sz parameter and decreases the Sa parameter. An obvious increase in the Sz parameter was observed with an increase in the incremental vertical step size.

Keywords: 2024-T3; aluminium alloy; incremental sheet forming; load-carrying capacity; surface finish; surface roughness



Citation: Trzepieciński, T.; Kubit, A.; Dzierwa, A.; Krasowski, B.; Jurczak, W. Surface Finish Analysis in Single Point Incremental Sheet Forming of Rib-Stiffened 2024-T3 and 7075-T6 Alclad Aluminium Alloy Panels. *Materials* **2021**, *14*, 1640. <https://doi.org/10.3390/ma14071640>

Academic Editor: Victor Songmene

Received: 24 February 2021

Accepted: 24 March 2021

Published: 27 March 2021

Publisher's Note: MDPI stays neutral with regard to jurisdictional claims in published maps and institutional affiliations.



Copyright: © 2021 by the authors. Licensee MDPI, Basel, Switzerland. This article is an open access article distributed under the terms and conditions of the Creative Commons Attribution (CC BY) license (<https://creativecommons.org/licenses/by/4.0/>).

1. Introduction

Appropriate selection of the parameters of the sheet metal forming process using single point incremental forming (SPIF) is intended to ensure appropriate surface quality in terms of roughness and, at the same time, an economically justified forming time [1,2]. The basic parameters in the process are: tool rotational speed, feed rate, step size, size and shape of the tool, type of sheet metal, and tool path [3–5]. The lubricant also plays a very important role. The surface roughness of the specimen is the result of the influence obtained between the tool and specimen, where the lubricant plays a significant role during

the forming process [6]. In order to optimise the process parameters, the Taguchi plan is often used [7–9]. Baruah et al. [10] conducted optimisation studies for the process of forming sheets of EN AW-5052 aluminium alloy using the Taguchi method. The results showed that effective lubrication is of the greatest importance for the formability and reduction of roughness in incremental sheet forming (ISF). Research on the influence of lubrication on surface quality was also carried out by Hussain et al. [11]. It was confirmed that the quality of the surface depends to a large extent on the properties of the lubricant and the method of its application.

One characteristic of the ISF forming process is the concentration of the deformation zone in the contact area of the tool face with the formed sheet. The size of this zone depends on the shape and size of the tool end and affects the formability of the sheet metal and its surface properties. Ham and Jeswiet [12,13] showed that a higher degree of formability is achieved with a smaller tool diameter due to the relatively large deformations concentrated in a small area of the material. Bhattacharya et al. [14] and Buff et al. [15] showed that tool rotational speed, feed rate and vertical step size have a significant impact on the formability of the ISFed sheets. Based on the experimental results, Ham and Jeswiet [12] claim that a low feed rate has a positive effect on sheet deformability. Vertical step size has a very significant influence on the formability and roughness of the shaped surface. Using the lowest possible step size values is recommended in order to obtain an appropriate surface quality [16–18]. Bhattacharya et al. [14] carried out research on the forming of EN AW-5052 aluminium alloy sheets and focussed on the effect of the step-down on the surface roughness of the draw piece surface. It was clearly indicated that an increase in the step size causes an increase in the surface roughness of the processed surface.

The investigations by Rubino et al. [19] and Andrade-Campos et al. [20] focussed on the strain distribution induced by the single point incremental forming of friction-stir-welded AA6082 sheets. It was found that in good-quality welds, material failure during SPIF occurs in the base material, evidencing that the mechanical properties of the welds are equal or better than those of the original material. Tucci et al. [21] developed an integrated numerical model able to simulate the manufacturing route for formed 6000 series aluminium alloy sheets welded by friction stir welding technology and finally shaped by means of a SPIF process. Thuillier et al. [22] performed the incremental forming of 6082-T6 aluminium alloy welded blanks until the fracture of truncated cones. The aim was to build an experimental database of the whole joining and forming process. Lu et al. [23] improved the surface quality of the parts by appropriately developing the tool path. A detailed review of the current state-of-the-art ISF processes in terms of their specific limitations, with discussions on the ISF process parameters and their effects on ISF processes, has been provided by Gatea et al. [24]. Rattanachan and Chungchoo [25] used the $2k-p$ factorial experimental design to analyse the interaction between the side overlap, step depth, tool feed rate and inner surface roughness. It was found that reducing tool rotational speed and feed rate reduced inner surface roughness.

In recent decades, artificial neural networks (ANNs) have become connections of elements called artificial neurons used to analyse complex regression problems [26–28]. There are many topologies of neural networks used to process the relationship between the explanatory and explained parameters [29,30]. Ambrogio et al. [31] proposed the implementation of ANN for predicting the geometrical variability of incrementally formed draw pieces. They also compared the Levenberg–Marquardt and backpropagation algorithms for predicting material failure. Kurra et al. [26] modelled the surface roughness in SPIF using ANNs and genetic programming. The optimum process parameters in SPIF were obtained and validated through these experiments, and highly satisfactory results were found with an error of less than 10%. Alsaman et al. [32] applied ANNs and the regression model to analyse the SPIF process for conical draw pieces. Najm and Paniti [4] used ANNs to predict the Ra and Rz parameters by adopting the data collected from frustum cones that were formed by SPIF. The results showed that an ANN with one argument in the output predicted the outcome sufficiently well when compared with a two-argument structure.

Oraon and Sharma [33] used the model of the ANN to predict the quality of the SPIF component's surface. The inputs were wall angle, feed rate, step size, sheet thickness, spindle speed and density of lubricant.

The research presented in the literature is mainly based on the SPIF of sheets that are not covered with a soft anticorrosion coating. The SPIF parameters should ensure the continuity of the protective layer after forming. This is especially important when forming sheets of high-strength EN AW-2024-T3 Alclad and EN AW-7075-T6 Alclad aluminium alloys commonly used in aircraft structures. The change in the thickness of the soft Alclad (technically pure aluminium) is related to the deformation of the core material and the mechanical interaction of the spherical end of the tool. Therefore, the SPIF process of Alclad sheets is different from that commonly studied in the literature, and in this paper, analysis is carried out on the change in surface roughness during the forming of rib-stiffened panels made of aluminium alloy Alclad sheets. The panels were formed using the single point incremental forming technique with a tool with a spherical end and a continuous spiral-shaped tool strategy. The load-carrying ability of rib-stiffened EN AW-2024-T3 and EN AW-7075-T6 aluminium alloy panels under axial compression has been studied in recent papers by the authors of [34,35]. In this paper, the effect of the forming parameters on the surface finish of the inner surface of stiffened ribs is studied based on experimental measurements of the surface roughness and on the artificial neural networks.

2. Materials and Methods

2.1. Material

Rib-stiffened panels were fabricated based on sheets with dimensions 160 mm × 120 mm (0.8-mm-thick EN AW-7075-T6 Alclad and 0.4-mm-thick EN AW-2024-T3 Alclad) and 160 mm × 100 mm (1-mm-thick EN AW-2024-T3). The chemical composition and the basic mechanical properties of the materials of the test sheets are shown in Tables 1 and 2, respectively.

Table 1. Chemical composition of test sheets in wt.% [36].

Alloy	Si	Fe	Mn	Cu	Mg	Cr	Zn	Ti	Other Elements		Al
									Each	Total	
2024-T3	0.50	0.50	0.3–0.9	3.8–4.9	1.2–1.8	0.10	0.25	0.15	0.05	0.15	Remainder
7075-T6	0.40	0.50	0.30	1.2–2.0	2.1–2.9	0.18–0.28	5.1–6.1	0.20	0.05	0.15	Remainder

Table 2. Basic mechanical properties of test sheets [36].

Material	Temper	Specified Thickness, mm		Tensile Strength R_m , MPa		Yield Stress $R_{p0.2}$, MPa		Elongation A_{50} min, %
		Over	Through	min	max	min	max	
EN AW-2024 Alclad	T3	0.25	0.50	405	-	270	-	12
EN AW-2024	T3	0.50	3.20	435	-	290	-	15
EN AW-7075 Alclad	T6	0.32	1.00	490	-	420	-	8

The tests were conducted in lubricated conditions using SAE 75W-85 gear oil supplied by Mannol (Wedel, Germany). About 5 mL of oil was used on each panel during the forming process. Basic physicochemical properties of the oil used are listed in Table 3.

Table 3. Basic physicochemical properties of SAE 75W-85 gear oil.

Density ρ (at 15 °C), kg/m ³	Flash Point, °C	Pour Point, °C	Viscosity at 40 °C, mm ² /s	Viscosity Index
879	210	−45	72.4	157

2.2. Forming Method

The ribs, with a width of 20 mm and an inner radius of 10 mm, were formed in the middle part of the panel (Figure 1a). During the experimental tests, 7 mm diameter hemispherical, high-speed HS2-9-2 steel was used for forming.

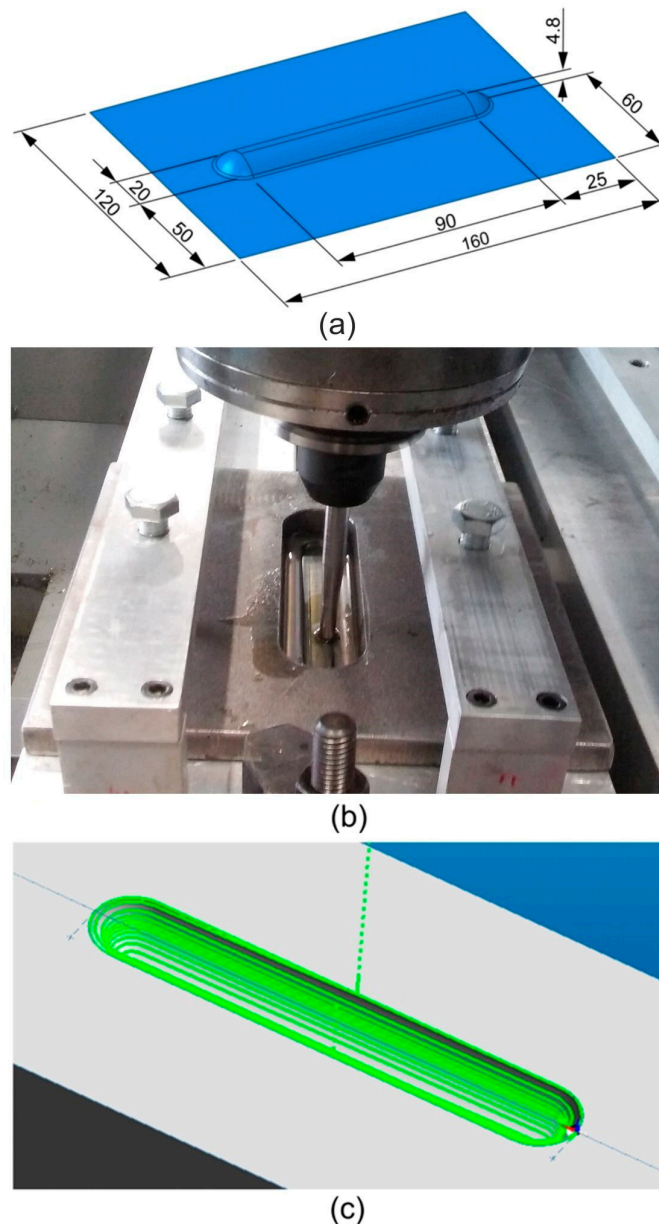


Figure 1. (a) Shape and dimensions of a rib-stiffened panel, (b) work-stand for single point incremental forming (SPIF) and (c) continuous spiral-shaped tool strategy generated in the EdgeCAM program.

The research was planned according to an orthogonal plan (two variable factors at three levels). A constant feed rate of 800 mm/min was used in the study. Incremental vertical step size a_p and tool rotational speed v (Table 4) were selected as variable parameters. The same research plan was applied to all the grades of sheet metals.

The device (supporting plate and blank holder) for SPIF was mounted on the table (Figure 1b) of a numerically controlled TM-1P vertical milling machine (Hass Automation, Oxnard, CA, USA). The sheet was placed between the supporting plate and the blank holder and clamped firmly at the edges using screws. During forming, the tool moves

in accordance with a path designed in the EdgeCAM program (Hexagon AB, Stockholm, Sweden). A continuous spiral-shaped toolpath (Figure 1c) was used in the investigations.

Table 4. Orthogonal array design.

Number of Experiment	Incremental Vertical Step Size a_p , mm	Tool Rotational Speed v , rpm
E1	0.2	18
E2	0.2	110
E3	0.2	202
E4	0.3	18
E5	0.3	110
E6	0.3	202
E7	0.4	18
E8	0.4	110
E9	0.4	202

2.3. Analysis of Surface Roughness

Scanning electron microscopy (SEM) was used to investigate wear on the inner surface of the formed ribs. Therefore, characterisation of the SEM samples was carried out on an S-3400 Phenom ProX SEM (Nanoscience Instruments, Phoenix, AZ, USA). Roughness measurements were performed by using a Talysurf CCI Lite white light interferometer (Taylor Hobson, Leicester, UK) with a vertical resolution of 0.01 nm. Basic 3D parameters of surface roughness were determined according to the ISO 25178-2 [37] standard. The profiles were taken perpendicular to the wear track in the middle part of the inner surface of the ribs (Figure 2).

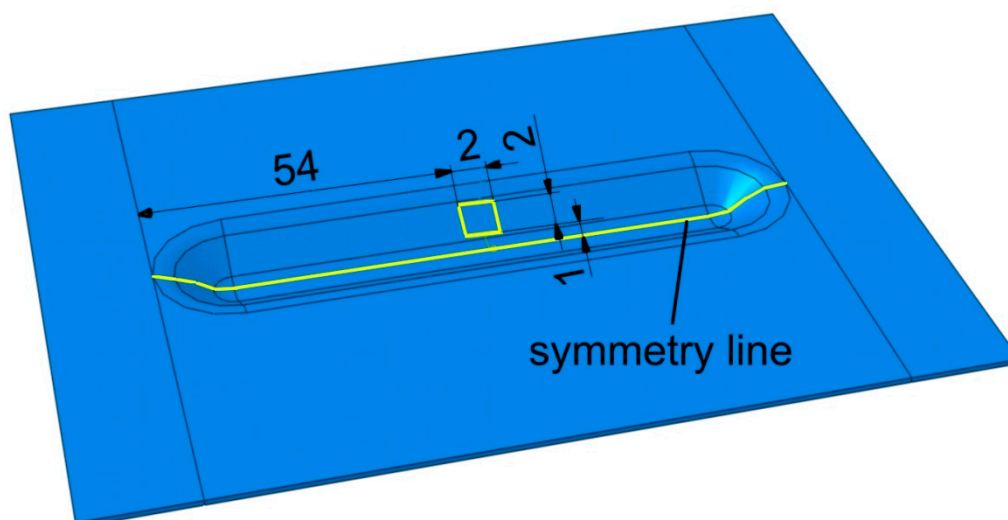


Figure 2. Location of measurement of the surface roughness in the inner surface of the stiffening ribs.

2.4. Artificial Neural Networks

The number of neurons in the input and output layers is determined by the number of parameters presented at the input and the number of parameters at the output. The Statistica program was used to analyse the effect of SPIF parameters on the surface roughness value of the stiffening ribs. The ANN algorithm (Intelligent Problem Solver) manuscript was built in the Statistica program, which automatically analyses the training set and possible correlations between input and output parameters for the specified number of multilayer perceptrons $n_a = 50$. Based on the results of this analysis, the structure of a neural network, which is optimal for the data in the training set, is proposed. The flowchart of the algorithm of the Intelligent Problem Solver module was not discussed

in the documentation of the Statistica program. The incremental vertical step size and the tool rotational speed were selected as explanatory parameters. The parameter to be explained was the arithmetical mean height Sa , the basic parameter of surface roughness in the machine manufacturing industry [38]. Due to the fact that sheets of various materials and thicknesses were tested, with or without the protective Alclad, it was decided to build an independent network for each of the sheets tested. It is possible to include all these parameters in one global network, but this requires the adding of new neurons at network input and, in consequence, could lead to the loss of the network's generalisation capabilities due to the limited amount of training data. While the number of neurons in the input and output layers is determined by the number of explanatory and explained variables, there are no general guidelines allowing a priori selection of the number of neurons in the hidden layer(s).

An ANN with a 2:2-8-1:1 structure (Figure 3) was selected after conducting a series of analyses with multilayer networks with a different number of neurons in the hidden layer based on the values of two parameters [39–42], i.e., the coefficient of determination R^2 (Equation (1)) and round mean square error RMSE (Equation (2)) for the analysis of the influence of SPIF parameters on the value of the average roughness Sa and the 10-point peak–valley surface roughness Sz of the inner surface of the stiffening ribs. Due to the small size of the training set, this network was used separately to forecast the values of the Sa and Sz parameters. Sa and Sz parameters are the most studied parameters of SPIFed surfaces [26]. The network shown in Figure 3 ensured the highest value of the determination coefficient R^2 and, at the same time, the lowest RMSE error for data contained in the training set. The values of the network quality parameters were determined as follows:

- Coefficient of determination, R^2 :

$$R^2 = 1 - \left(\frac{\sum_{i=1}^n (a_j - p_j)^2}{\sum_{i=1}^n (p_j)^2} \right) \quad (1)$$

- Round mean square error, RMSE:

$$RMSE = \sqrt{\frac{1}{n} \sum_{i=1}^n |a_j - p_j|^2} \quad (2)$$

where a is the actual value, p is the predicted value and n is the number of training sets.

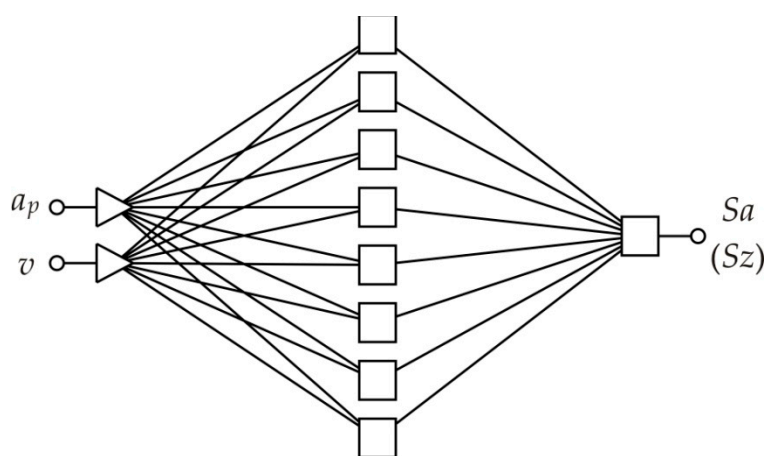


Figure 3. The architecture of the network used to analyse the effect of SPIF parameters on the value of the Sa roughness parameter.

The training of the network was carried out with the use of various algorithms, which provided comparable results for the relatively uncomplicated network used in the investigations.

3. Results

3.1. Surface Topography

Selected surface topographies and the values of the basic parameters of the stereometric structure of the inner surface of the ribs formed in 1-mm-thick EN AW-2024-T3, 0.4-mm-thick EN AW-2024-T3 Alclad and 0.8-mm-thick EN AW-7075-T6 aluminium alloy sheets are shown in Figures 4–6 and Table 5.

It was found that the inner surface of the ribs revealed small linear ridges as a result of the interaction of the spherical-shaped tool tip with the workpiece. The greater the value of the incremental vertical step size, the more prominent the ridges (1-mm-thick EN AW-2024-T3—Figure 4a, 0.8-mm-thick EN AW-7075-T6 Alclad—Figure 5a and 0.4-mm-thick EN AW-2024-T3 Alclad—Figure 6a). Because the difference between the lowest valley and the highest peak on the surface is S_z , the tool tip is continuously cultivating the sheet surface and creating new grooves. When the incremental vertical step size a_p is small, then the grooves are continuously plastically deformed, and one can even detect flattening of the surface. The grooves presented in Figures 4b, 5b and 6b correspond to the 1-mm-thick EN AW-2024-T3, 0.8-mm-thick EN AW-7075-T6 Alclad and 0.4-mm-thick EN AW-2024-T3 Alclad, respectively. The asperities on the sheet surface are destroyed and recreated continuously by the topography of the tool. In the case of Alclad sheets (Figures 5 and 6), there is no clear effect of the tool rotational speed on the arrangement and pitch of ridges. However, when forming the EN AW-2024-T3 sheets without Alclad, the highest tool rotational speed caused tearing of the lateral sides of ridges (Figure 4c). A similar effect was observed when forming sheets with Alclad (Figures 5c and 6c). In the case of 1-mm-thick EN AW-2024-T3 sheets, the increase in the vertical step size a_p under constant tool rotational speed leads to an increase in the S_z parameter (Table 5). There are no other clear relationships within the specific grade of sheet metal. The relations between a_p and v affecting it are imperceptible due to small differences in the values of parameters. Therefore, it is necessary to build a model that takes the overall view on the change in surface roughness into account. This will be the topic of the next chapter.

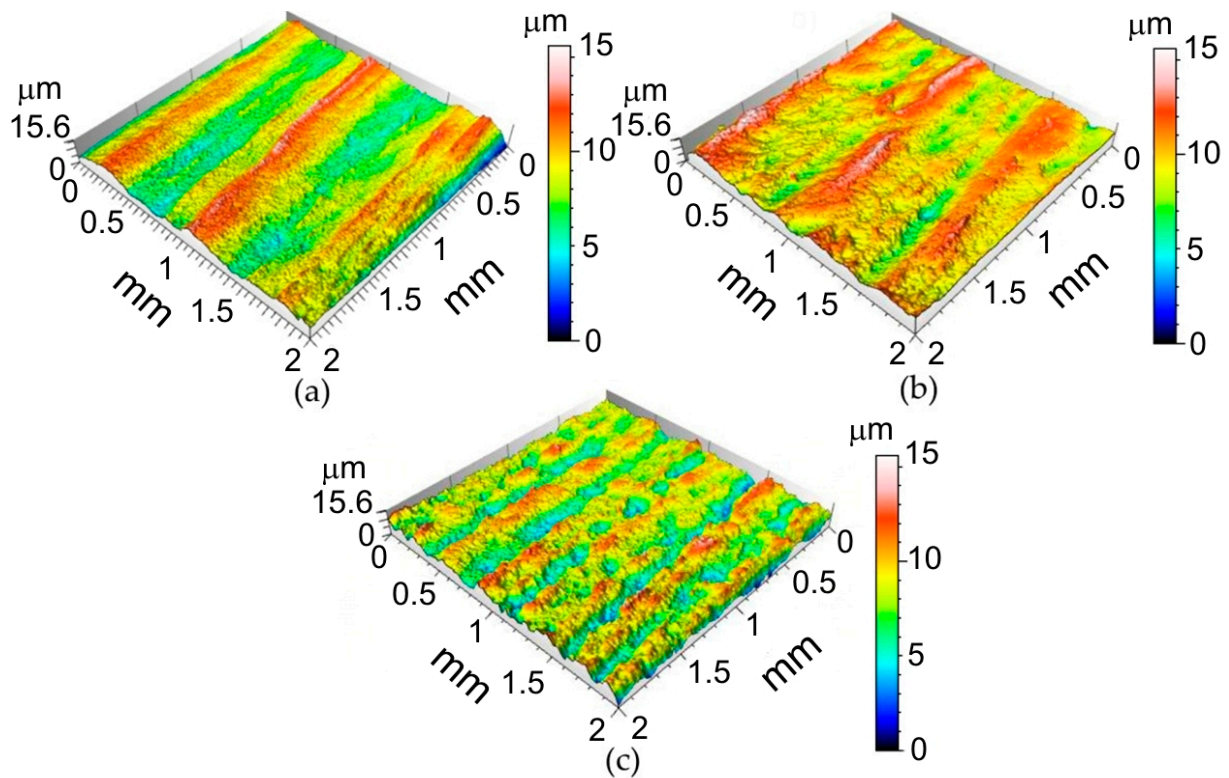


Figure 4. Surface topographies of the inner surface of ribs formed in 1-mm-thick EN AW-2024-T3 fabricated with the following conditions: (a) $a_p = 0.4$ mm, $v = 18$ rpm; (b) $a_p = 0.4$ mm, $v = 202$ rpm; (c) $a_p = 0.2$ mm, $v = 202$ rpm.

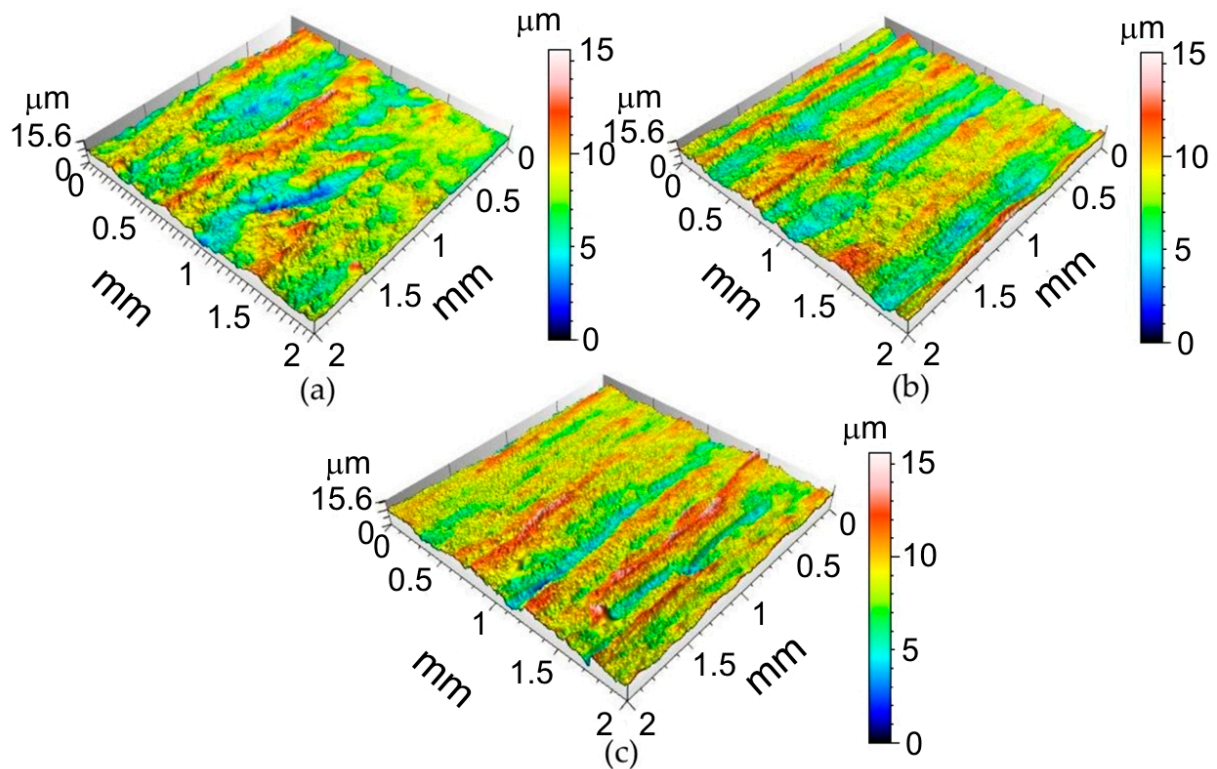


Figure 5. Surface topographies of the inner surface of ribs formed in 0.8-mm-thick EN AW-7075-T6 Alclad fabricated with the following conditions: (a) $a_p = 0.4$ mm, $v = 18$ rpm; (b) $a_p = 0.4$ mm, $v = 202$ rpm; (c) $a_p = 0.2$ mm, $v = 202$ rpm.

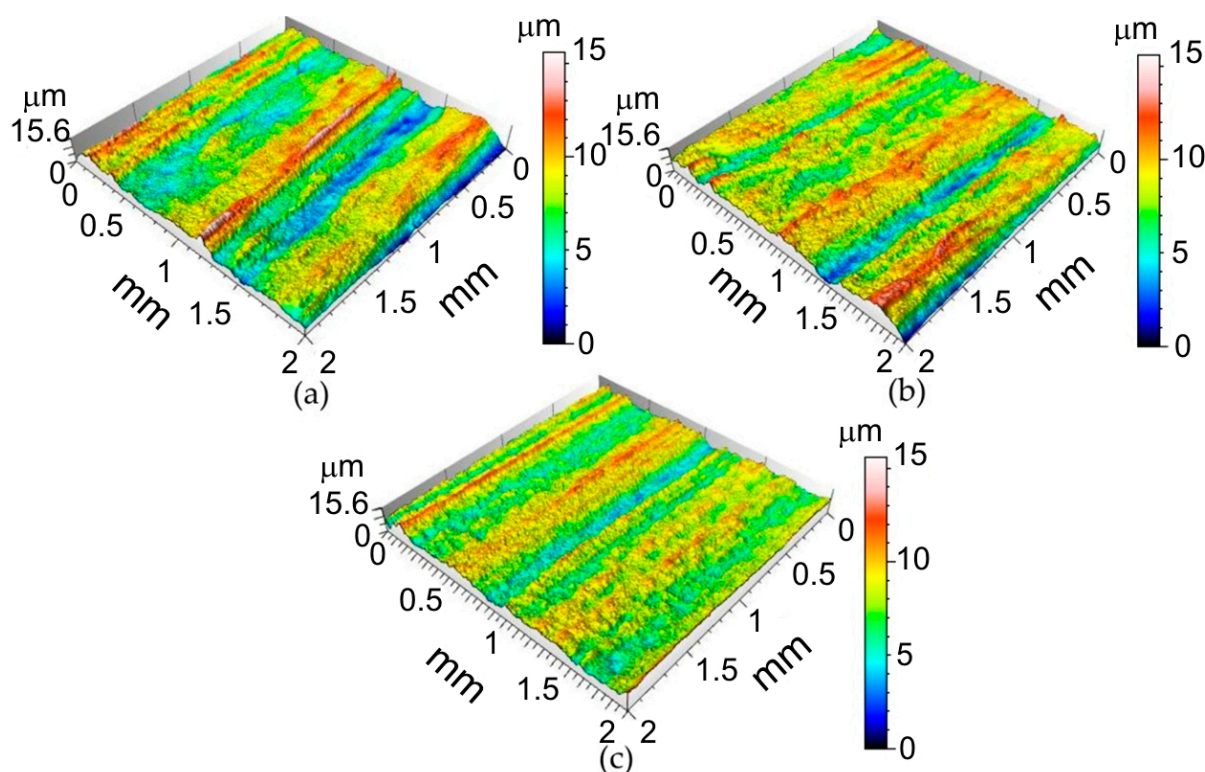


Figure 6. Surface topographies of the inner surface of ribs formed in 0.4-mm-thick EN AW-2024-T3 Alclad fabricated at with the following conditions: (a) $a_p = 0.4$ mm, $v = 18$ rpm; (b) $a_p = 0.4$ mm, $v = 202$ rpm; (c) $a_p = 0.2$ mm, $v = 202$ rpm.

Table 5. Basic amplitude parameters of the surface roughness of the ribs formed in 1-mm-thick EN AW-2024-T3 sheets.

a_p , mm	v , rpm	Sq , μm	Ssk	Sku	Sp , μm	Sv , μm	Sz , μm	Sa , μm
0.2	18	1.09	0.355	3.10	5.16	4.33	9.49	0.874
	110	0.94	0.0009	2.73	3.85	3.69	7.54	0.733
	202	0.99	−0.0872	2.60	4.05	4.30	8.36	0.799
0.3	18	1.16	−0.321	3.37	3.86	4.67	8.53	0.914
	110	1.53	0.0228	2.45	5.09	4.77	9.86	1.26
	202	0.93	−0.184	3.50	3.34	4.91	8.25	0.737
0.4	18	1.92	0.192	2.65	7.12	8.51	15.6	1.59
	110	1.19	0.0649	3.35	4.93	6.65	11.6	0.940
	202	1.39	−0.0958	3.69	4.88	8.29	13.2	1.09

3.2. ANN Modelling

The training of the network was carried out with the use of various algorithms (quasi-Newton, backpropagation and Levenberg–Marquardt), which provided comparable results for the relatively uncomplicated network used in the investigations. The learning process was characterised by a continuous reduction of the network error along with an increase in the number of epochs, during which the training data were presented to the network. The learning process was carried out until there was no further reduction of the network error [42]. The values of the network for individual learning algorithms and the number of learning epochs necessary to achieve the minimum value of the error function are presented in Table 6. The smallest error values were observed for networks learned with the quasi-Newton algorithm. The number of learning epochs necessary to reach the minimum error value was about 80 for the quasi-Newton algorithm, 140 for the backpropagation algorithm and 170 for the network trained using the Levenberg–Marquardt algorithm.

Table 6. RMSEs for the 2:2-8-1:1 networks trained using different algorithms.

Sheet Material	Output Variable	RMSE for Training Set		
		Quasi-Newton	Back Propagation	Levenberg–Marquardt
0.4-mm-thick EN AW-2024-T3 Alclad	<i>Sa</i>	0.1206	0.1278	0.1381
	<i>Sz</i>	0.4624	0.4821	0.4997
0.8-mm-thick EN AW-7075-T6 Alclad	<i>Sa</i>	0.3004	0.3189	0.3047
	<i>Sz</i>	0.0817	0.0974	0.1086
1-mm-thick EN AW-2024-T3	<i>Sa</i>	0.2860	0.3068	0.3091
	<i>Sz</i>	0.1311	0.1457	0.1531

So, in this paper, the variable metric (quasi-Newton) algorithm was selected to present the results of the training process. The quasi-Newton algorithm ensures the fastest achievement of the error minimum by the network response during the learning process [43,44]. From the training set, 20% of the cases were randomly selected and assigned to the validation set, which is used for independent control of the training algorithm. The validation set protects the learning process against “Occam’s razor”, according to which “in explaining phenomena one should strive for simplicity, choosing such explanations that are based on the fewest assumptions and concepts”. Failure to meet Occam’s condition leads to overfitting of the network to the training data, and, consequently, its ability to generalise the data is lost. RMSE error values for the networks are shown in Table 6. The differences in the values of these errors for different networks result from the difference in the possible data noise in the training sets. Another explanation for the differences is the different character of interaction of the spherically ended tool with a clad and an unclad sheet surface. Alclad is an aluminium alloy core material metallurgically bonded to a high-purity aluminium surface layer, which, due to reduced hardness, is much more susceptible to roughening than the core metal. Another explanation for the differences in errors is due to random selection by the learning algorithm of data that were qualified to the validation set. Removal of data that carried significant information from the training set could reduce the quality of the training process.

The observation of changes in the value of the network learning error is a response to a possible network training error, while next to the network learning error, very important parameters indicating the network’s approximation abilities are the coefficient of determination and the mean of the absolute error. Taking into account the small amount of training data, all networks were characterised by a relatively high value of the coefficient of determination defined for the training set (Tr. SA in Figure 7) above $R^2 = 0.657$ (Figure 7a–c). Values of the standard deviation ratio above 0.512 for the training set indicate an average quality of the predictive neural network.

The coefficient of determination of neural networks with *Rz* as the explained variable was characterised by a high value of the coefficient of determination $R^2 > 0.92$ (Figure 7d–f). This means that the input parameters correlate more closely with the roughness parameter *Sz* than with the *Sa* parameter. Moreover, the networks explaining the value of the *Sa* parameter were characterised by an about two times lower value of the standard deviation ratio. The lower the value of this coefficient, the better the quality of the model constructed.

	Tr. SZ		Tr. SZ		Tr. SZ
Data Mean	0.396361	Data Mean	0.7382397	Data Mean	0.5095289
Data S.D.	0.3706392	Data S.D.	0.3850771	Data S.D.	0.3248869
Error Mean	-0.05026	Error Mean	0.1293778	Error Mean	-0.2017
Error S.D.	0.2841315	Error S.D.	0.2928821	Error S.D.	0.2190582
Abs E. Mean	0.2058558	Abs E. Mean	0.2617742	Abs E. Mean	0.2135158
S. D. Ratio	0.7665988	S. D. Ratio	0.7605805	S. D. Ratio	0.6742597
Correlation	0.7085505	Correlation	0.6774437	Correlation	0.8514288
(a)		(b)		(c)	
	Tr. SZ		Tr. SZ		Tr. SZ
Data Mean	0.4959964	Data Mean	0.4489278	Data Mean	0.330292
Data S.D.	0.3594278	Data S.D.	0.3701268	Data S.D.	0.1988191
Error Mean	-0.4571	Error Mean	-0.01681	Error Mean	0.06318
Error S.D.	0.07429	Error S.D.	0.1390066	Error S.D.	0.05552
Abs E. Mean	0.4571441	Abs E. Mean	0.1166942	Abs E. Mean	0.07136
S. D. Ratio	0.2067011	S. D. Ratio	0.3755649	S. D. Ratio	0.2792594
Correlation	0.9799598	Correlation	0.9272062	Correlation	0.9616543
(d)		(e)		(f)	

Figure 7. Basic regression parameters of the artificial neural networks modelling the effect of process parameters on roughness parameters S_a (a–c) and S_z (d–f): (a,d) 0.4-mm-thick EN AW-2024-T3 Alclad, (b,e) 1-mm-thick EN AW-2024-T3 and (c,f) 0.8-mm-thick EN AW-7075-T6 Alclad: Data S.D.—standard deviation of data, Error S.D.—error of standard deviation, Abs. E. Mean—absolute error mean, S.D. Ratio—standard deviation ratio, Correlation—coefficient of determination R^2 .

The principal goal of the analyses carried out with the use of neural networks, apart from an attempt to build a high-quality network based on a relatively small set of training data, was to find out the relationship between the parameters of the SPIF process and the value of the average roughness S_a . The response surfaces of the neural networks for the data concerning all materials are shown in Figure 8. According to all neural models, increasing the value of the incremental vertical step size ap increases the value of the surface roughness parameter S_a . The influence of the tool rotation speed v on the value of the S_a parameter is more complex. When forming sheets with an Alclad (Figure 8a,c), increasing the rotational speed v reduces the value of the average roughness S_a parameter. A reverse relationship can be observed for the EN AW-2024-T3 sheet (Figure 8b) which did not have a protective anticorrosive coating. This can be explained by the heating of the soft Alclad containing a large proportion of pure aluminium, under the adhesive effect of the surface of the rotating tool. Consequently, the plasticised asperities of the sheet surface were more susceptible to flattening.

It was found that during the forming of ribs in Alclad sheets there is a clear relationship between the average roughness S_a and the 10-point peak–valley surface roughness S_z . Increasing the rotational speed of the tool and vertical step size increases the value of the parameter S_a (Figure 9a,c) and the parameter S_z (Figure 9a,c). In the case of the sheet not being covered by soft Alclad, the reduction of tool rotational speed increases the S_z parameter (Figure 9b) and reduces the S_a parameter (Figure 8b). So, the tool rotational speed is a more important parameter in determining the surface finish than incremental vertical step size. In the case of sheets covered by a soft layer of technically pure aluminium, the inner surface of the ribs was more easily ploughed. So, the pronounced directional scratches can be easily correlated with the change of parameters S_a and S_z . The character of the interaction of the hard surface of the spherically shaped tools with the relatively high-strength of the surface of the greatest thickness (1 mm) of the EN AW-2024-T3 aluminium alloy sheet causes the deformation of the surface asperities. These changes take place in cyclical ridges so the surface asperities are flattened without significant changes in the depths of the valleys.

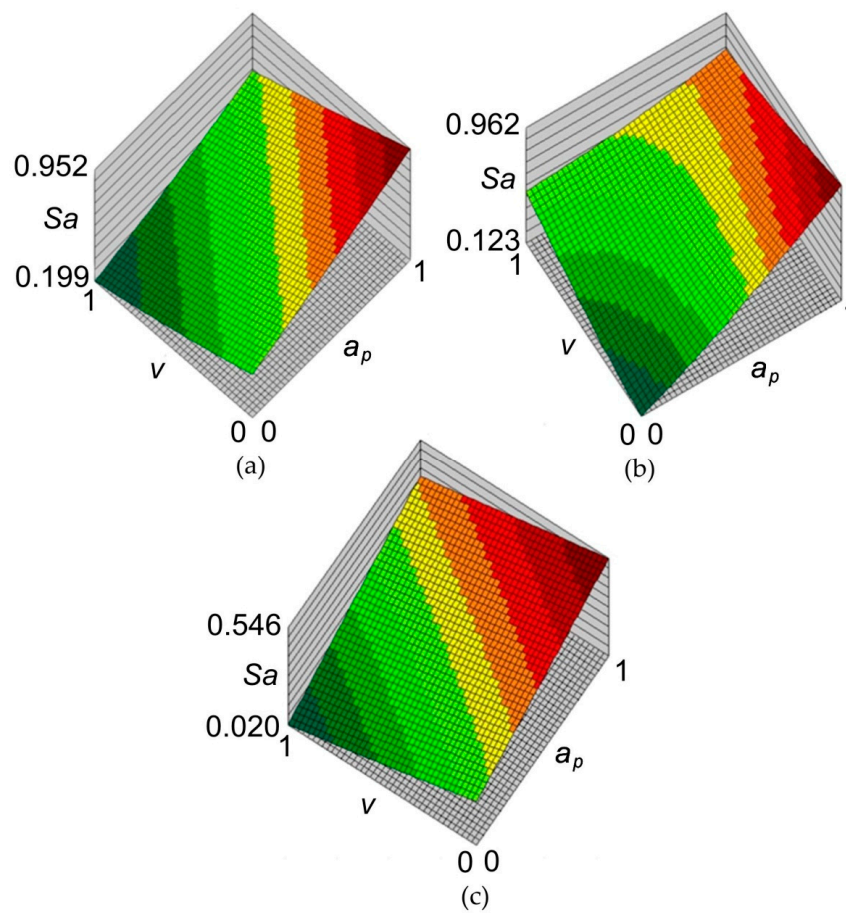


Figure 8. Response surfaces of the neural network 2:2-8-1:1 concerning the influence of incremental vertical step size a_p and the tool rotational speed v on the value of the average roughness Sa (normalised data) for sheets: (a) 0.4-mm-thick EN AW-2024-T3 Alclad, (b) 1-mm-thick EN AW-2024-T3 and (c) 0.8-mm-thick EN AW-7075-T6 Alclad.

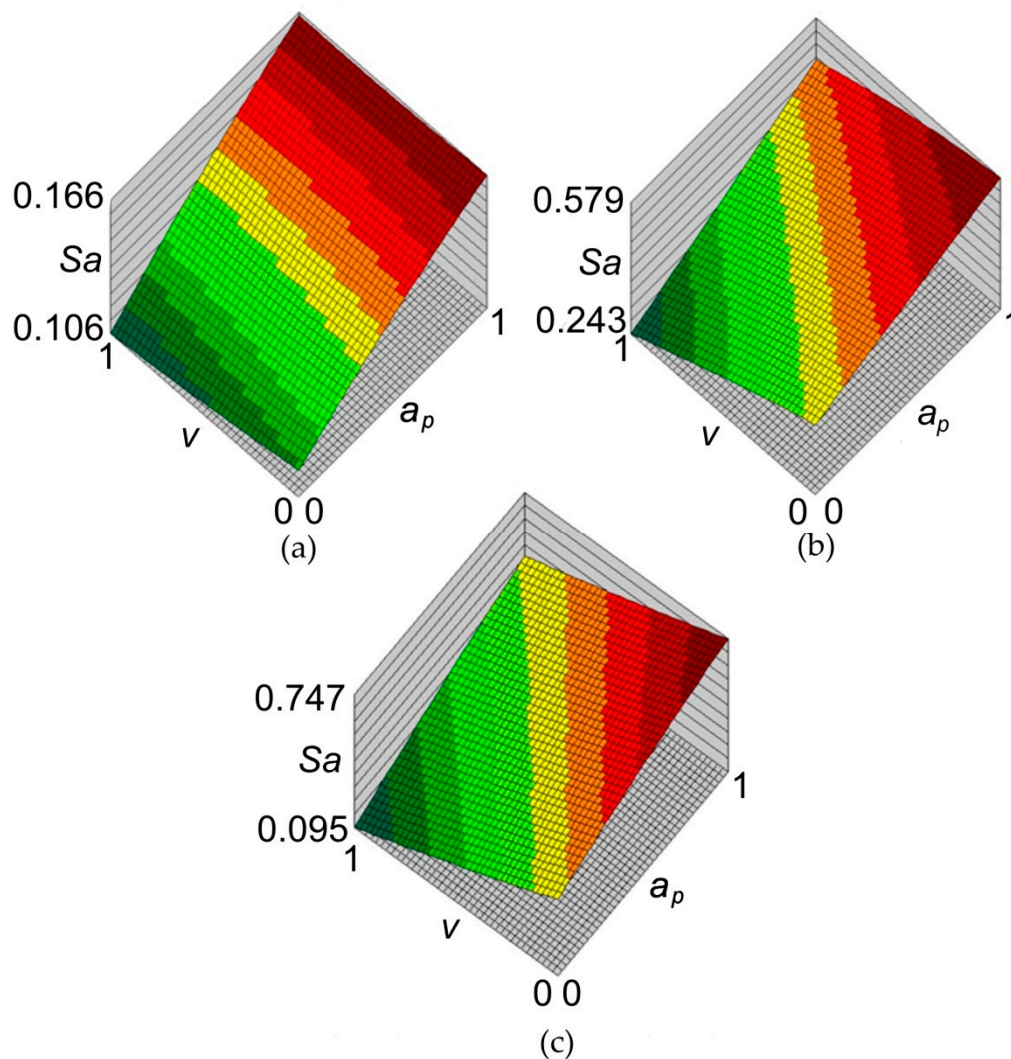


Figure 9. Response surfaces of the neural network 2:2-8-1:1 concerning the influence of incremental vertical step size a_p and the tool rotational speed v on the value of the 10-point peak–valley surface roughness S_z (normalised data) for sheets: (a) 0.4-mm-thick EN AW-2024-T3 Alclad, (b) 1-mm-thick EN AW-2024-T3 and (c) 0.8-mm-thick EN AW-7075-T6 Alclad.

4. Conclusions

In this paper, an analysis is presented on the effect of SPIF parameters on the surface roughness of stiffened ribs formed in EN-2024-T3 and EN AW-7075-T6 aluminium alloy sheets with and without the high-purity aluminium surface layers metallurgically bonded to the core material. The following conclusions are drawn from the experimental research and ANN analyses:

- The greater the value of the incremental vertical step size, the more prominent the ridges found in the inner surface of stiffened ribs, especially in the case of both Alclad aluminium alloy sheets.
- In the case of Alclad sheets, there is no clear effect of the tool rotational speed on the arrangement and pitch of ridges. However, when forming the 1-mm-thick EN AW-2024-T3 sheets (without Alclad), the highest tool rotational speed caused tearing of the lateral sides of the ridges.
- Regardless of the grade of the sheet, an obvious increase in the S_z parameter was observed with an increase in the incremental vertical step size.

- The performance measures of the multilayer perceptrons predicting the values of average roughness Sa and the 10-point peak–valley surface roughness Sz ranges between 0.657 and 0.979, respectively.
- Alclad sheets exhibit a different character of changes of parameters Sa and Sz from unclad sheets. In the case of Alclad sheets, increasing the value of the incremental vertical step size increases the value of the surface roughness parameters Sa and Sz . The reduction of the tool rotational speed increases the Sz parameter and decreases the Sa parameter when forming unclad sheets.

Author Contributions: Conceptualization, B.K., A.K. and T.T.; methodology, B.K. and A.K.; software, A.D. and W.J.; validation, A.K., T.T. and W.J.; formal analysis, W.J.; investigation, B.K., A.K., T.T. and A.D.; data curation, A.K., A.D. and T.T.; writing—original draft preparation, T.T.; writing—review and editing, T.T. All authors have read and agreed to the published version of the manuscript.

Funding: This research received no external funding.

Institutional Review Board Statement: Not applicable.

Informed Consent Statement: Not applicable.

Data Availability Statement: The data presented in this study are available on request from the corresponding author.

Conflicts of Interest: The authors declare no conflict of interest.

References

1. Jagtap, R.; Kashid, S.; Kumar, S.; Hussein, H.M.A. An experimental study on the influence of tool path, tool diameter and pitch in single point incremental forming (SPIF). *Adv. Mater. Process. Technol.* **2015**, *1*, 465–473. [\[CrossRef\]](#)
2. Khalil, U.; Aziz, M.H.; Jahanzaib, M.; Ahmad, W.; Hussain, S.; Hafeez, F. Effects of forming tools and process parameters on surface roughness in incremental sheet forming. *Adv. Sci. Technol. Res. J.* **2018**, *12*, 75–95. [\[CrossRef\]](#)
3. Liu, Z.; Li, Y. Small data-driven modeling of forming force in single point incremental forming using neural networks. *Eng. Comput.* **2020**, *36*, 1589–1597. [\[CrossRef\]](#)
4. Najm, S.M.; Paniti, I. Predict the Effects of Forming Tool Characteristics on surface roughness of aluminum foil components formed by SPIF using ANN and SVR. *Int. J. Precis. Eng. Manuf.* **2021**, *22*, 13–26. [\[CrossRef\]](#)
5. Sisoida, V.; Kumar, S. Influence of process parameters on surface roughness in single point incremental forming using dummy sheet. *IOP Conf. Ser. Mater. Sci. Eng.* **2018**, *361*, 012003. [\[CrossRef\]](#)
6. Sornsuwit, N.; Sittisakuljaroen, S. The effect of lubricants and material properties in surface roughness and formability for single point incremental forming process. *Adv. Mater. Res.* **2014**, *979*, 359–362. [\[CrossRef\]](#)
7. Chinnaiyan, P.; Jeevanantham, A. Multi-objective optimization of single point incremental sheet forming of AA5052 using Taguchi based grey relational analysis coupled with principal component analysis. *Int. J. Precis. Eng. Manuf.* **2014**, *15*, 2309–2316. [\[CrossRef\]](#)
8. Kurra, S.; Regalla, S. Multi-objective optimisation of single point incremental sheet forming using Taguchi-based grey relational analysis. *Int. J. Mater. Eng. Innov.* **2015**, *6*, 74–90. [\[CrossRef\]](#)
9. Uttarwar, P.; Raini, S.; Malwad, D. Optimization of process parameter on surface roughness (Ra) and wall thickness on SPIF using Taguchi method. *Int. Res. J. Eng. Technol.* **2015**, *2*, 781–784.
10. Baruah, A.; Pandivelan, C.; Jeevanantham, A.K. Optimization of AA5052 in incremental sheet forming using grey relational analysis. *Measurement* **2017**, *106*, 95–100. [\[CrossRef\]](#)
11. Hussain, G.; Gao, L.; Hayat, N.; Cui, Z.; Pang, Y.C.; Dar, N.U. Tool and lubrication for negative incremental forming of a commercially pure titanium sheet. *J. Mater. Process. Technol.* **2008**, *203*, 193–201. [\[CrossRef\]](#)
12. Ham, M.; Jeswiet, J. Single point incremental forming and the forming criteria for AA3003. *CIRP Ann. Manuf. Technol.* **2006**, *55*, 241–244. [\[CrossRef\]](#)
13. Ham, M.; Jeswiet, J. Forming limit curves in single point incremental forming. *CIRP Ann. Manuf. Technol.* **2007**, *56*, 277–280. [\[CrossRef\]](#)
14. Bhattacharya, A.; Maneesh, K.; Venkata Reddy, N.; Cao, J. Formability and surface finish studies in single point incremental forming. *J. Manuf. Sci. Eng.* **2011**, *133*, 061020. [\[CrossRef\]](#)
15. Buffa, G.; Campanella, D.; Fratini, L. On the improvement of material formability in SPIF operation through tool stirring action. *Int. J. Adv. Manuf. Technol.* **2013**, *66*, 1343–1351. [\[CrossRef\]](#)
16. Hussain, G.; Gao, L.; Zhang, Z. Formability evaluation of a pure titanium sheet in the cold incremental forming process. *Int. J. Adv. Manuf. Technol.* **2008**, *37*, 920–926. [\[CrossRef\]](#)

17. Attanasio, A.; Ceretti, E.; Giardini, C.; Mazzoni, L. Asymmetric two points incremental forming: Improving surface quality and geometric accuracy by tool path optimization. *J. Mater. Process. Technol.* **2008**, *197*, 59–67. [[CrossRef](#)]
18. Hagan, E.; Jeswiet, J. Analysis of surface roughness for parts formed by computer numerical controlled incremental forming. *J. Eng. Manuf.* **2004**, *218 Pt B*, 1307–1312. [[CrossRef](#)]
19. Rubino, F.; Esperto, V.; Paulo, R.M.F.; Tucci, F.; Carlone, P. Integrated manufacturing of AA6082 by friction stir welding and incremental forming: Strain analysis of deformed samples. *Procedia Manuf.* **2020**, *47*, 440–444. [[CrossRef](#)]
20. Andrade-Campos, A.; Thuillier, S.; Martins, J.; Carlone, P.; Tucci, F.; Valente, R.; Paulo, R.M.F.; Alves de Sousa, R.J. Integrated design in welding and incremental forming: Material model calibration for friction stir welded blanks. *Procedia Manuf.* **2020**, *47*, 429–434. [[CrossRef](#)]
21. Tucci, F.; Valente, R.A.F.; Alves de Sousa, R.J.; Rubino, F.; Carlone, P. A finite element approach to the integrated modelling of the incremental forming of friction stir welded sheets. *AIP Conf. Proc.* **2019**, *2113*, 060005.
22. Thuillier, S.; Andrade-Campos, A.; Carlone, P.; Valente, R.; Alves de Sousa, R.J. Integrated design in welding and incremental forming: Mechanical behavior off riction stir welded blanks. *AIP Conf. Proc.* **2019**, *2113*, 060010.
23. Lu, B.; Chen, J.; Ou, H.; Cao, J. Feature-based tool path generation approach for incremental sheet forming process. *J. Mater. Process. Technol.* **2013**, *213*, 1221–1233. [[CrossRef](#)]
24. Gatea, S.; Ou, H.; McCartney, G. Review on the influence of process parameters in incremental sheet forming. *Int. J. Manuf. Technol.* **2016**, *87*, 479–499. [[CrossRef](#)]
25. Rattanachan, K.; Chungchoo, C. The effected of single point incremental forming process parameters on the formed part surface roughness. *Adv. Mater. Res.* **2014**, *979*, 335–338. [[CrossRef](#)]
26. Kurra, S.; Rahman, N.H.; Regalla, S.P.; Gupta, A.K. Modeling and optimization of surface roughness in single point incremental sheet forming process. *J. Mater. Res. Technol.* **2015**, *4*, 304–313. [[CrossRef](#)]
27. Lemu, H.G.; Trzepieciński, T. Multiple regression and neural network based characterization of friction in sheet metal forming. *Adv. Mater. Res.* **2014**, *1051*, 204–210. [[CrossRef](#)]
28. Trzepieciński, T.; Lemu, H.G. Effect of activation function and post synaptic potential on response of artificial neural network to predict frictional resistance of aluminium alloy sheets. *IOP Sci. Conf. Ser. Mater. Sci. Eng.* **2017**, *269*, 012041. [[CrossRef](#)]
29. Altaf, S.; Mehmood, M.S.; Imran, M. Implementation of efficient artificial neural network data fusion classification technique for induction motor fault detection. *J. Eng. Sci.* **2018**, *5*, E16–E21. [[CrossRef](#)]
30. Rao, K.V.; Murthy, B.S.N.; Rao, M. Prediction of cutting tool wear, surface roughness and vibration of work piece in boring of AISI 316 steel with artificial neural network. *Measurement* **2014**, *51*, 63–70.
31. Ambrogio, G.; Filice, L.; Guerriero, F.; Guido, R.; Umbrello, D. Prediction of incremental sheet forming process performance using a neural network approach. *Int. J. Adv. Manuf. Technol.* **2011**, *54*, 921–930. [[CrossRef](#)]
32. Alsamhan, A.; Ragab, A.E.; Dabwan, A.; Nasr, M.M.; Hidri, L. Prediction of formation force during single-point incremental sheet metal forming using artificial intelligence techniques. *PLoS ONE* **2019**, *14*, e0221341. [[CrossRef](#)]
33. Oraon, M.; Sharma, V. Prediction of surface roughness in single point incremental forming of AA3003-O alloy using artificial neural network. *Int. J. Mater. Eng. Innov.* **2018**, *9*, 1–19. [[CrossRef](#)]
34. Kubit, A.; Wydrzyński, D.; Bucior, M.; Krasowski, B. Testing of stiffening ribs formed by incremental forming in thin-walled aircraft structures made of 2024-T3 Alclad aluminium alloy. *AIP Conf. Proc.* **2018**, *1960*, 160015.
35. Slota, J.; Kubit, A.; Trzepieciński, T.; Krasowski, B.; Varga, J. Ultimate load-carrying ability of rib-stiffened 2024-T3 and 7075-T6 aluminium alloy panels under axial compression. *Materials* **2021**, *14*, 1176. [[CrossRef](#)]
36. ASTM B209M-14. Standard Specification for Aluminum and Aluminum-Alloy Sheet and Plate. ASTM International: West Conshohocken, PA, USA, 2014.
37. ISO 25178-2:2012 Geometrical Product Specifications (GPS)—Surface Texture: Areal—Part 2: Terms, Definitions and Surface Texture Parameters; ISO: Geneva, Switzerland, 2012.
38. Sedlaček, M.; Podgornik, B.; Vižintin, J. Influence of surface preparation on roughness parameters, friction and wear. *Wear* **2009**, *266*, 482–487. [[CrossRef](#)]
39. Cagan, S.C.; Aci, M.; Buldum, B.B.; Aci, C. Artificial neural networks in mechanical surface enhancement technique for the prediction of surface roughness and microhardness of magnesium alloy. *Bull. Polish Acad. Sci. Tech. Sci.* **2019**, *67*, 729–739.
40. Esme, U.; Sagbas, A.; Kahraman, F.; Kulekci, M.K. Use of artificial neural networks in ball burnishing process for the prediction of surface roughness of AA 7075 aluminium alloy. *Mater. Technol.* **2008**, *42*, 215–219.
41. Nalbant, M.; Gökkaya, H.; Toktaş, I.; Sur, G. The experimental investigation of the effects of uncoated, PVD- and CVD-coated cemented carbide inserts and cutting parameters on surface roughness in CNC turning and its prediction using artificial neural networks. *Robot. Comp. Integr. Manuf.* **2009**, *25*, 211–223. [[CrossRef](#)]
42. Trzepieciński, T.; Gelgele, H.L. Application of genetic algorithm for optimization of neural networks for selected tribological test. *Acta Mech. Slovaca* **2012**, *16*, 54–60. [[CrossRef](#)]
43. Hagan, M.T.; Menhaj, M.B. Training feedforward networks with the Marquardt algorithm. *IEEE Trans. Neural Netw.* **1994**, *5*, 989–993. [[CrossRef](#)] [[PubMed](#)]
44. Marquardt, D. An algorithm for least squares estimation of non-linear parameters. *J. Soc. Ind. Appl. Math.* **1963**, *11*, 431–441. [[CrossRef](#)]